Hindawi Publishing Corporation
Journal of Aerodynamics
Volume 2014, Article ID 678518, 13 pages
http://dx.doi.org/10.1155/2014/678518

Research Article

Drag Reduction of Passenger Car Using Add-On Devices

Ram Bansal[1] and R. B. Sharma[2]

[1] *Department of Automobile Engineering, RJIT BSF Academy, Tekanpur, India*
[2] *Mechanical Engineering Department, RJIT BSF Academy, Tekanpur, India*

Correspondence should be addressed to Ram Bansal; rambansal37@gmail.com

Received 12 July 2013; Revised 15 December 2013; Accepted 15 December 2013; Published 23 March 2014

Academic Editor: Noor A. Ahmed

This work proposes an effective numerical model using the Computational Fluid Dynamics (CFD) to obtain the flow structure around a passenger car with different add-on devices. The computational/numerical model of the passenger car and mesh was constructed using ANSYS Fluent which is the CFD solver and employed in the present work. In this study, numerical iterations are completed, and then aerodynamic data and detailed complicated flow structure are visualized. In the present work, a model of generic passenger car was developed using solidworks, generated the wind tunnel, and applied the boundary conditions in ANSYS workbench platform, and then testing and simulation have been performed for the evaluation of drag coefficient for passenger car. In another case, the aerodynamics of the most suitable design of vortex generator, spoiler, tail plates, and spoiler with VGs are introduced and analysed for the evaluation of drag coefficient for passenger car. The addition of these add-on devices are reduces the drag-coefficient and lift coefficient in head-on wind. Rounding the edges partially reduces drag in head-on wind but does not bring about the significant improvements in the aerodynamic efficiency of the passenger car with add-on devices, and it can be obtained. Hence, the drag force can be reduced by using add-on devices on vehicle and fuel economy, stability of a passenger car can be improved.

1. Introduction

A few years ago when the fuel crisis was not a problem, cars were mainly designed for high-speed manoeuvrability, comfort, and safety. However, since 2002 with the recent impact of increasing fuel prices the decreasing sales of automobiles have crippled the industry all over the world. This was immediately followed by many questions raised regarding the effect of oil supply shortage on the future of this industry. Many solutions were certainly suggested and many once-considered-infeasible solutions were now given serious consideration. Besides the development of electric cars and fuel cells, other proposed approaches include the integration of air conditioning systems with electronic devices to cut down energy consumption, the redesign of car frames and bodies to reduce the total weight, and the modification of car bodies to improve the overall aerodynamic characteristics for improved cruising conditions, reliable of navigation and lower energy consumption. These improvements are also indirectly related to the environment and noise pollution.

In the process of car design, the aerodynamics must be seriously considered. A car design can, generally, only be acceptable if its form drag is reduced to a set target. Many researchers have made use of CFD techniques [1–4] to perform numerical simulations related to automobile aerodynamics.

The current study presents the development process of aerodynamic holography of the vehicle outer body. Several numerical simulations were performed to analyse the pressure field, velocity vector field, and aerodynamic force prediction related to a passenger car. Then, the stability of the aerodynamic forces caused by the airflow over the car was examined. Thereafter, the installation of add-on devices that leads to lower aerodynamic drag was carefully evaluated. Through Fluent [5, 6], this work used the k-ε turbulence model in a steady-state flow to compute the flow field around the car and its add-on devices.

As a matter of fact, it is very uncommon to use k-ε turbulence model in an iteration-dependent [7] problem. However, it is the goal of this work to demonstrate the feasibility of

Figure 1: Experimental setup of wind tunnel.

integrating this very uncommon approach (i.e., the using of k-ε turbulence model) in this type of computational model. Within a relatively short amount of time, this computational process was capable of estimating the aerodynamics of a car with high accuracy. This will provide automobile research and development teams with an alternative approach when performing CAE analysis.

In general, the design criteria of add-on devices are only limited to aerodynamic considerations. Car drivers usually install add-on devices that successfully reduce the lift and improve traction leading to manoeuvrability and stability. However, the aerodynamics performance corresponding to the add-on devices could deteriorate severely. For this reason, this work aims to target designers of car add-on devices to provide a new tool or an idea for an add-on device design process. In the following sections, the methodology will be presented in detail.

2. Methodology

In this work, first of all a generic model of the passenger car is prepared in the Solidworks software and this generic model is imported into the ANSYS Fluent to do the simulation of the coefficient of drag and coefficient of lift in the wind tunnel which is generated in the design module of the ANSYS Fluent. After this the meshing is generated on the surface of the passenger car.

Aerodynamic evaluation of airflow over an object can be performed using analytical method or CFD approach. On one hand, analytical method of solving airflow over an object can be done only for simple flows over simple geometries like laminar flow over a flat plate. If airflow gets complex as in flows over a bluff body, the flow becomes turbulent and it is impossible to solve Navier-Stokes and continuity equations analytically. On the other hand, obtaining direct numerical solution of Navier-stoke equation is not yet possible even with modern day computers. In order to come up with reasonable solution, a time averaged Navier-Stokes equation is being used (Reynolds Averaged Navier-Stokes Equations (RANS) equations) together with turbulent models to resolve the issue involving Reynolds stress resulting from the time averaging process.

In the present work the k-ε turbulence model with non-equilibrium wall function is selected to analyze the flow over the generic passenger car model. This k-ε turbulence model is very robust, having reasonable computational turnaround time, and widely used by the autoindustry.

Table 1

Type	Open type wind tunnel
Test section	150 × 150 × 750 mm
Blower	Compatible capacity
Motor	3HP AC Motor Crompton make with AC Drive ABB make
Speed controller	For variable seed
Air velocity	Maximum 30 m/s (in test section)
Digital force indicator	Lift force up to 11 kg, drag force up to 11 kg
Multiple manometers	13 PVC tubes, 0–40° inclination with vertical axis
U Tube manometer	Length 1 m
Inclined manometer	300 mm
Pitot static tube	For velocity measurement
Micro-Pitot tube	For boundary layer experiment

Table 2

Configurations	Drag coefficient (C_D)	Lift coefficient (C_L)
Toy Car	0.3497	0.2289

3. Experimental Setup

Figure 1 shows the experimental setup of the wind tunnel at which we have performed the experiment on a toy car to deduce the drag coefficient and lift coefficient.

The specifications of the wind tunnel are given in Table 1.

4. Experimental Analysis

For values of C_D and C_L of toy car, see Table 2.

After experiment we have got the coefficient of drag (C_D) is 0.3497 and coefficient of lift (C_L) that is 0.2289.

5. Steps for Simulation

(i) Select the models of vehicle upon which add-on devices are to be used.

(ii) Formation of baseline model: design a model in solid works with proper dimensions and parameters.

(iii) Baseline passenger car CFD method and setup: apply the boundary conditions.

(iv) Generate the wind tunnel for simulation.

(v) Simulate and test the baseline passenger car for drag coefficient and lift coefficient.

(vi) Simulate and test the passenger car with vortex generators for drag coefficient and lift coefficient.

(vii) Simulate and test the passenger car with spoiler for drag coefficient and lift coefficient.

(viii) Simulate and test the passenger car with tail plates for drag coefficient and lift coefficient.

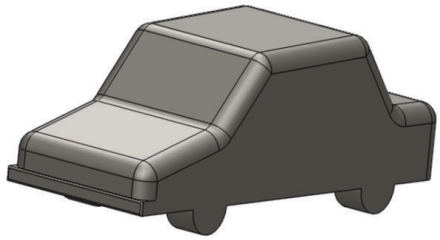

Figure 2: Solid-work model of car without VGs.

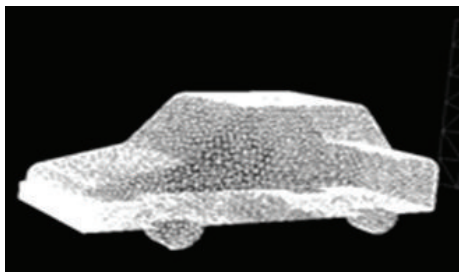

Figure 3: Meshed model of base car.

(ix) Simulate and test the passenger car with spoiler and vortex generators together for drag coefficient and lift coefficient.

(x) Impact of add-on device on fuel economy of passenger car.

6. Formation of Baseline Model

The baseline model of generic passenger car is designed in solid works. Figure 2 shows the generic passenger car used in the present CFD simulation. The full size generic passenger car is 375 mm long, 80 mm wide, and 60 mm high.Thereafter, this model has been analysed for drag coefficient and forces under the ANSYS (Fluent) module and values of drag coefficient and lift coefficient.

The surface mesh of generic passenger car is shown in Figure 3. The tetrahedrons type meshing is generated on its surface. A surface mesh of 1.5 mm size is created on the vehicle surface (Figure 4).

7. Baseline Passenger Car CFD Method and Setup

The CFD simulation by Yang and Khalighi [8] is reproduced in the present simulation. Tables 3, 4, 5, and 6 show the solver setup, viscous model, and turbulence model settings, boundary condition settings, and solution controls for present simulation, respectively. The assumptions made in present simulation have the airflow steady state with constant velocity at inlet and with zero degree yaw angle, constant pressure outlet, no slip wall boundary conditions at the vehicle surfaces, and inviscid flow wall boundary condition on the top, sidewalls, and ground face of the virtual wind tunnel (Figures 7, 9, 10, and 11).

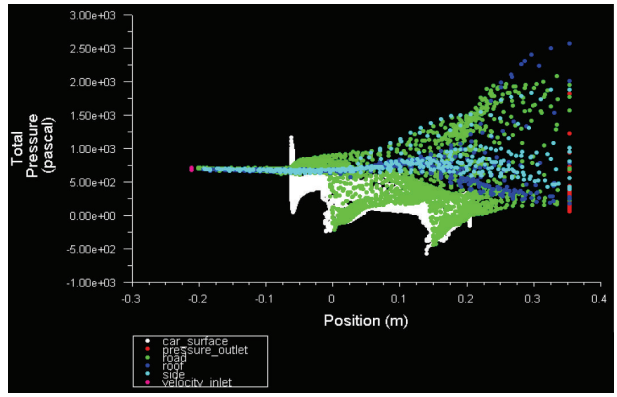

Figure 4: Total pressure on car surface, velocity inlet, pressure outlet, and road of base model.

Table 3: Solver setting.

CFD simulation	3d dp (3D double precision)
Solver	
Solver	Fluent
Space	3D
Formulation	Implicit
Time	Steady
Velocity formulation	Absolute
Gradient option	Cell-based
Porous formulation	Superficial velocity

Table 4: Viscous model and Turbulence model settings.

Turbulence model	k-ε (2 eqn)
k-ε model	Standard
Near-wall treatment	Enhanced wall function
Operating conditions	Ambient

8. Simulation and Testing of Baseline Passenger Car for Drag Coefficient and Lift Coefficient

Figure 8 shows the pressure coefficient plot on the car surface for base model simulation. The pressure coefficient plot shows that the stagnation point is created on the front surface of the passenger car. The pressure coefficient also indicates that CFD simulations have a tendency to overshoot the C_P value at stagnation point. The maximum C_P value obtained in base model simulation is $C_P = 2.0$.

Figures 5 and 6 show the coefficients of drag (C_D) and coefficients of lift (C_L) on the base model. Maximum value of the coefficient of drag is 0.3512 and the maximum value of the coefficient of lift is 0.2310.

9. Values of C_D and C_L of Baseline Model

After simulation we have got that the coefficient of drag (C_D) is 0.3512 and coefficient of lift (C_L) is 0.2310 (see Table 7).

Table 5: Boundary condition settings.

Boundary conditions		
Velocity inlet	Magnitude (measured normal to boundary)	22 m/s (constant)
	Turbulence specification method	Intensity and Viscosity Ratio
	Turbulence intensity	1.00%
	Turbulence viscosity ratio	20
Pressure outlet	Gauge pressure magnitude	0 Pa
	Gauge pressure direction	normal to boundary
	Turbulence specification method	Intensity and viscosity ratio
	Backflow turbulence intensity	10%
	Backflow turbulent viscosity ratio	10
Wall zones	(i) Vehicle surface-no slip wall B/c (ii) Ground face-inviscid wall B/C (iii) Side faces-inviscid wall B/C	
Fluid properties	Fluid type	Air
	Density	$\rho = 1.175$ (kg/m^3)
	Kinematic viscosity	$\nu = 1.7894 \times 10^{-5}$ (kg/(m·s))

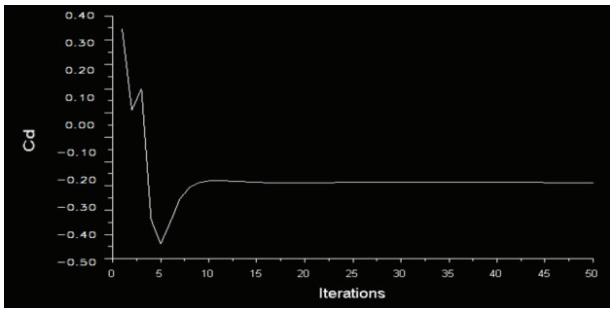

Figure 5: Drag coefficients C_D of base model.

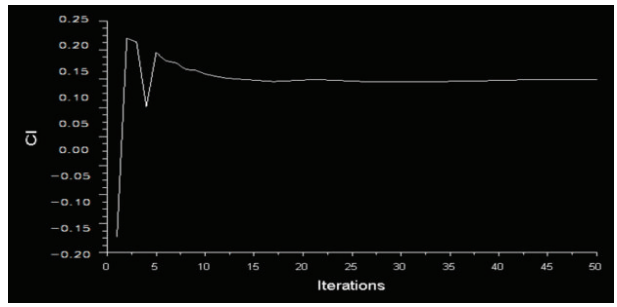

Figure 6: Lift coefficients C_L of base model.

Table 6: Solution controls.

Equations	Flow and turbulence
Discretization	(i) Pressure: standard (ii) Momentum: second order upwind (iii) Turbulence kinetic energy: second order upwind (iv) Turbulence dissipation rate: second order upwind
Monitor	Residuals and drag coefficient
Convergence Criterion	(i) Continuity = 0.001 (ii) X-velocity = 0.001 (iii) Y-velocity = 0.001 (iv) k = 0.001 (v) Epsilon = 0.001

Table 7

Configurations	Drag coefficient (C_D)	Lift coefficient (C_L)
Baseline	0.3512	0.2310

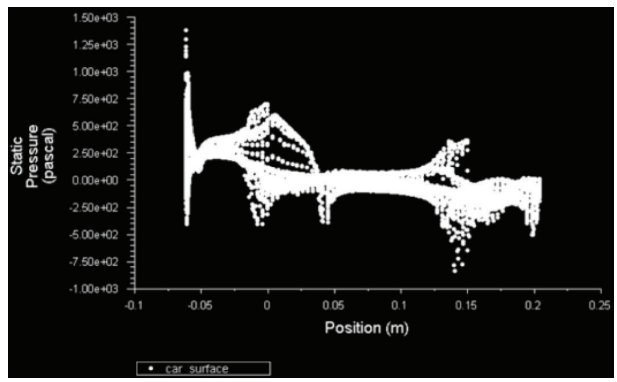

Figure 7: Static pressure distributions on base model car surface.

10. Result Validation

We have analysed that the percentage difference of drag coefficient and lift coefficient b/w of the toy car and base model is 0.3 and 0.9, respectively, which is less than 1%. So we assume that our model is the same as the specimen toy car (see Table 8).

Table 8

Configurations	Drag coefficient (C_D)	% C_D reduction from toy car	Lift coefficient (C_L)	% C_L reduction from toy car
Toy car	0.3497	0	0.2289	0
Base model	0.3512	0.3	0.2310	0.9

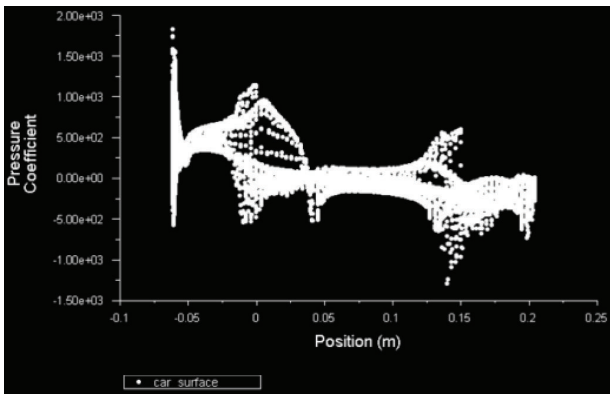

Figure 8: Pressure coefficient on base model car surface.

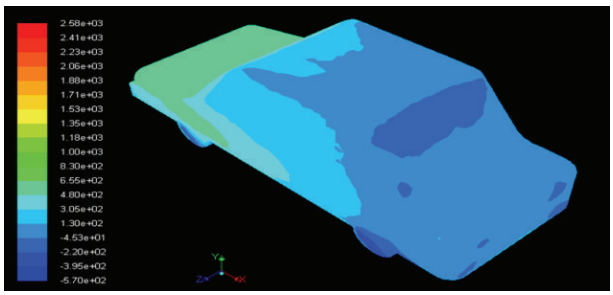

Figure 9: Total pressure on surface of the of base model passenger car.

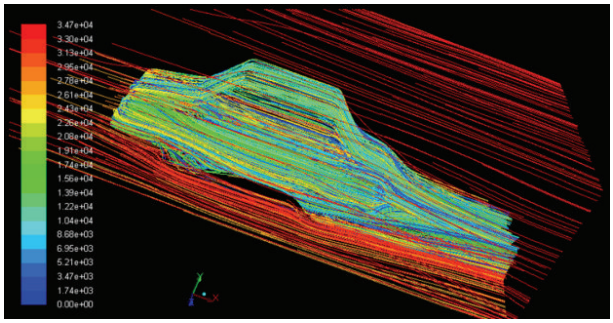

Figure 10: Path lines on surface of the of base model passenger car.

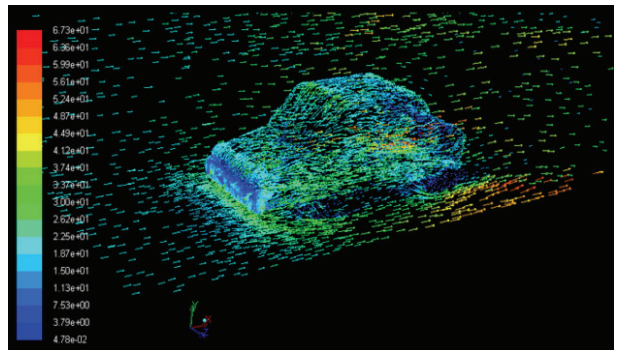

Figure 11: Velocity vector on surface of the of base model passenger car.

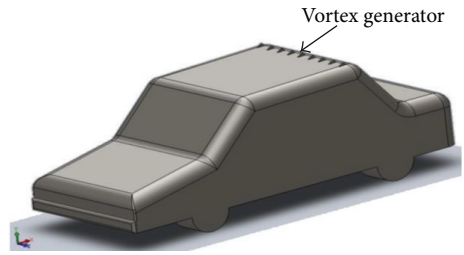

Figure 12: Passenger car with vortex generators.

11. Simulation and Testing of Passenger Car with Vortex Generators for Drag Coefficient and Lift Coefficient

First, a background on vehicle aerodynamics will be covered, including explanation of the concepts and formulas involved. Next, the procedure for building a basic model, including the passenger car and wind tunnel, along with dimensions and simulation parameters, will be developed. The basic model will then be compared with a reputable benchmark to confirm validity of the simulation setup and corresponding results. Once the basic simulation model is benchmarked, it will then be modified to include the external drag reduction devices. Two different VG designs will be studied, which include a delta wing design and bump-shaped design. Once the basic VG design is established, the next step will be to experiment with difference VG heights in order to determine the ideal height for the passenger car model. CFD simulations will be performed on the modified models to examine the results and determine the changes.

The vortex generators are placed at the backside of the roof of the passenger car which is shown in Figure 12.

Figure 13 shows the total pressure distribution on surface of the generic passenger car, velocity inlet, pressure outlet, and on road.

The coefficient of drag and coefficient of lift are shown in Figures 14 and 15, respectively. The maximum value of the coefficient of drag (C_D) is 0.3471 and the maximum value of the coefficient of lift (C_L) is 0.2085.

Figures 16 and 17 are show the static and absolute pressure distribution on the surface of the car.

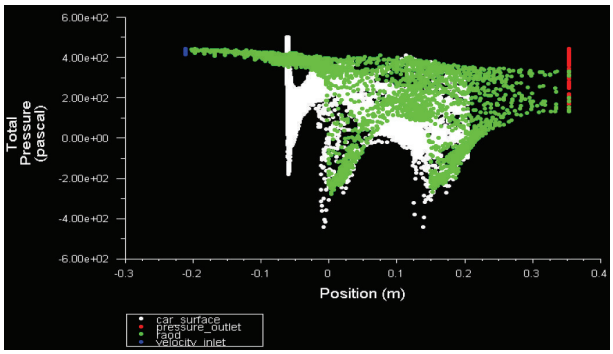

FIGURE 13: Total pressure distributions at car surface, pressure outlet, velocity inlet, and road.

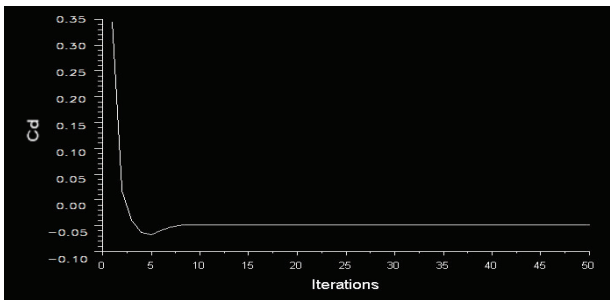

FIGURE 14: Coefficient of drag C_D of passenger car with VGs.

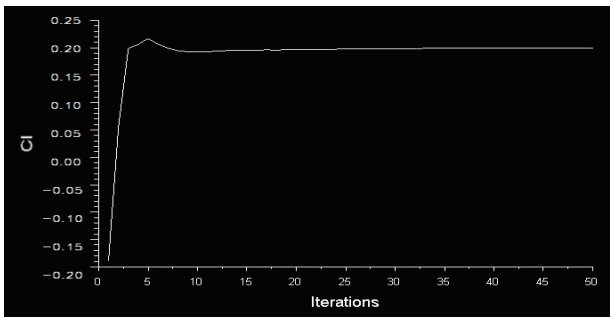

FIGURE 15: Coefficient of lift C_L of passenger car with VGs.

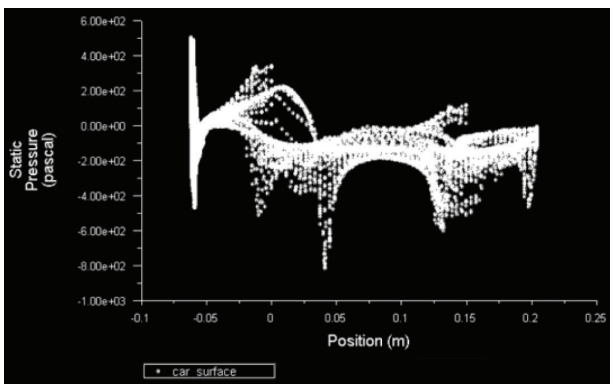

FIGURE 16: Static pressure distributions on car surface with VGs.

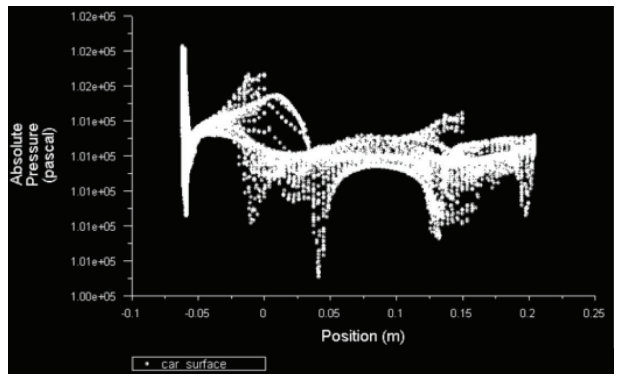

FIGURE 17: Absolute pressure distributions on car surface with VGs.

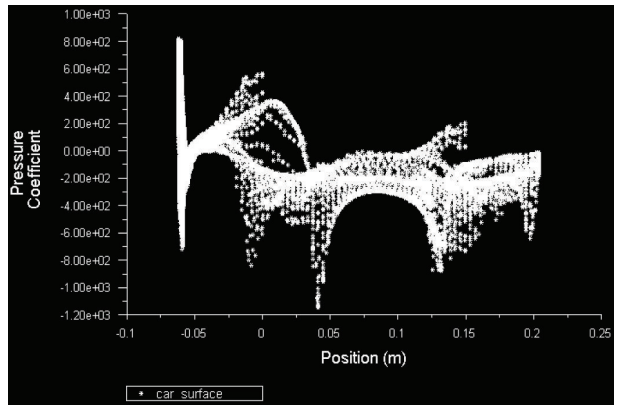

FIGURE 18: Pressure coefficient of car surface with VGs.

The distribution of the pressure coefficient on the car surface is shown in Figure 18.The value of pressure coefficient on the front bumper is 900 Pa and at the rear boot the value of the pressure coefficient is −200 Pa.

Total pressure contour and velocity contour are shown in Figures 19 and 20, respectively. The path lines and velocity magnitude vector are shown in Figures 21, 22, and 23.

12. Simulation and Testing of Passenger Car with Spoiler for Drag Coefficient and Lift Coefficient

A Spoiler, 15 cm long, is attached to the boot of the car at an inclination angle of 12° as shown in Figure 24. It is expected that the spoiler will delay the separation of flow that normally occurs at the rear edge of the boot.

Figure 25 shows the mesh generated on the surface of the model of generic passenger car with spoiler. The tetrahedron mesh is generated on its surface and a surface mesh of 1.5 mm size is created on the vehicle surface.

Figure 26 shows the total pressure distribution on the car surface, velocity inlet, pressure outlet, side wall, and on the road. The distribution of pressure on the front bumper is 1100 Pa and at the rear boot is 400 Pa as shown.

The coefficient of drag and coefficient of lift are shown in Figures 27 and 28, respectively. The maximum value of

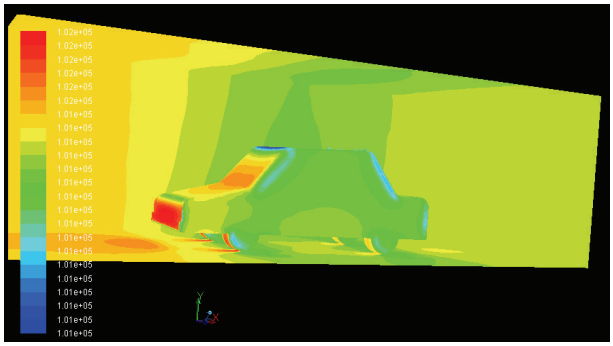

Figure 19: Total pressure contour on car surface, symmetry, and road.

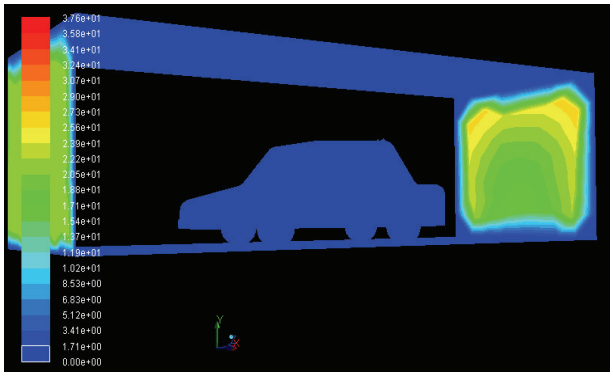

Figure 20: Velocity contour on car surface, velocity inlet, pressure outlet, and road.

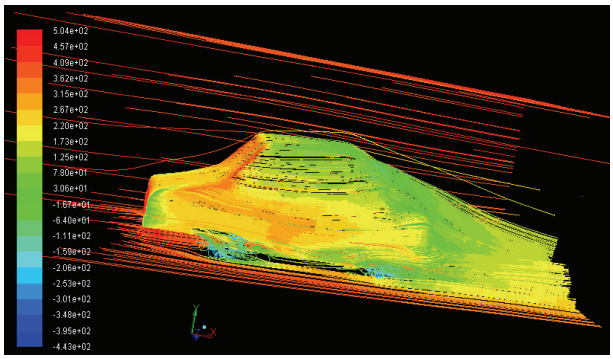

Figure 21: Pressure path lines on car surface and symmetry.

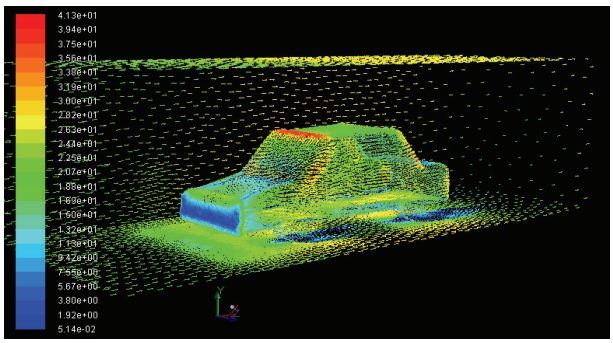

Figure 22: Velocity vector on the car surface, symmetry, and road.

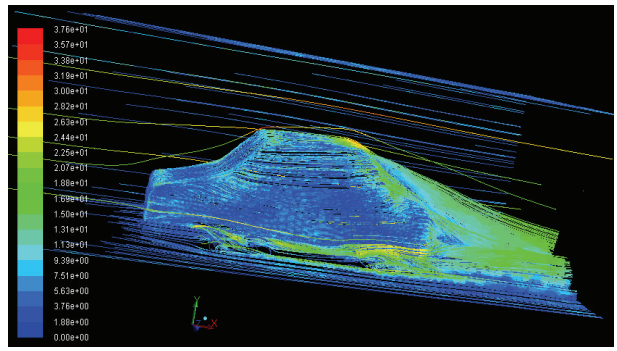

Figure 23: Velocity path lines on car surface, symmetry, and road.

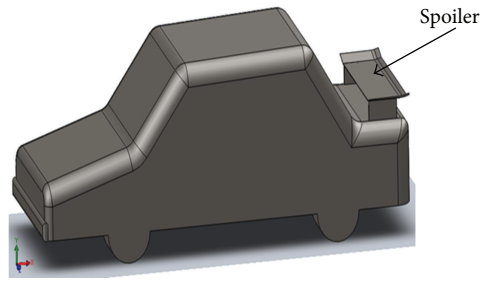

Figure 24: Passenger car with the attached spoiler.

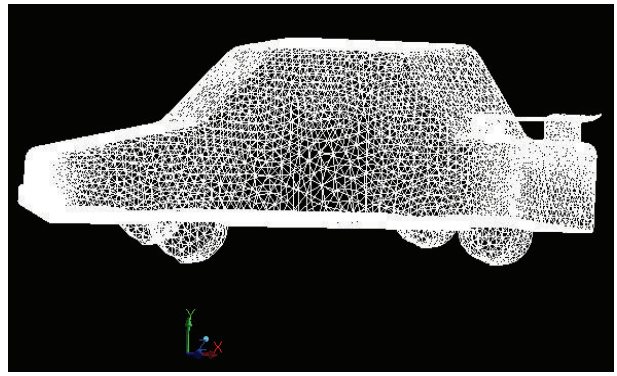

Figure 25: Meshed model of car with spoiler.

the coefficient of drag (C_D) is 0.3441 and the maximum value of the coefficient of lift (C_L) is 0.1985.

Figures 29 and 30 show the static and absolute pressure distributions on the surface of the car. The different values of the pressure distribution on the car surface such as front bonnet, roof, and rear boot are shown.

The distribution of the pressure coefficient on the car surface is shown in Figure 31. The value of pressure coefficient on the front bumper is 1750 Pa and at the rear boot the value of the pressure coefficient is 100 Pa.

Total pressure contour and velocity contour are shown in Figures 32 and 33, respectively. The velocity magnitude vector and path lines are shown in Figures 34 and 35, respectively.

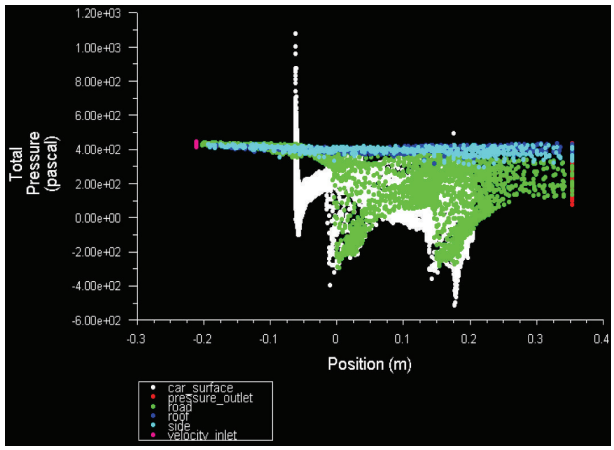

Figure 26: Total pressure distributions at car surface, pressure outlet, velocity inlet, and road.

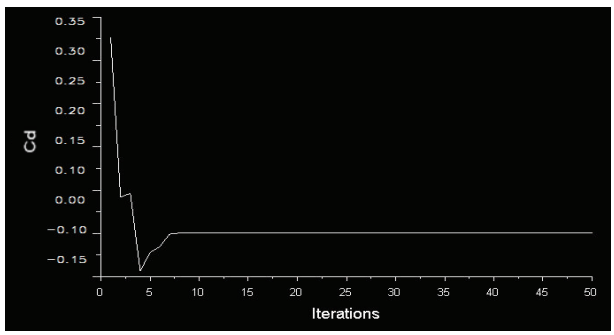

Figure 27: Coefficient of drag C_D of passenger car with spoiler.

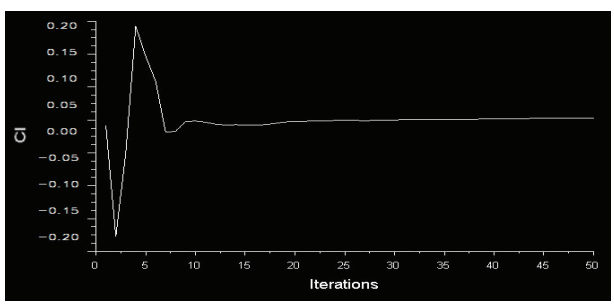

Figure 28: Coefficient of lift C_L of passenger car with spoiler.

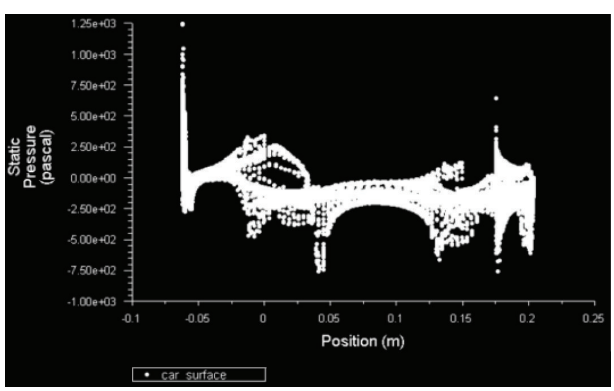

Figure 29: Static pressure distributions on car surface with spoiler.

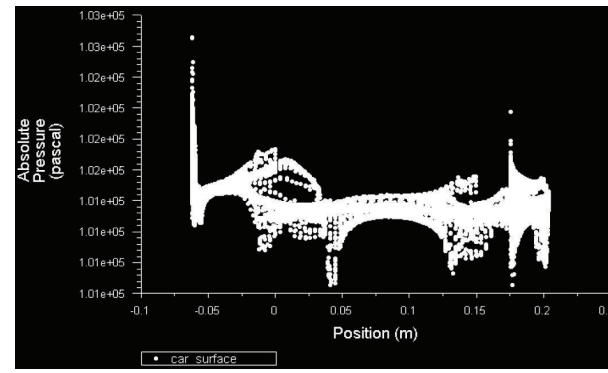

Figure 30: Absolute pressure distributions on car surface with Spoiler.

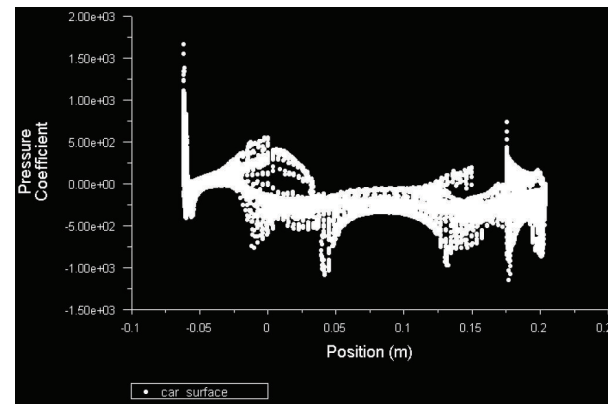

Figure 31: Pressure coefficient on car surface with spoiler.

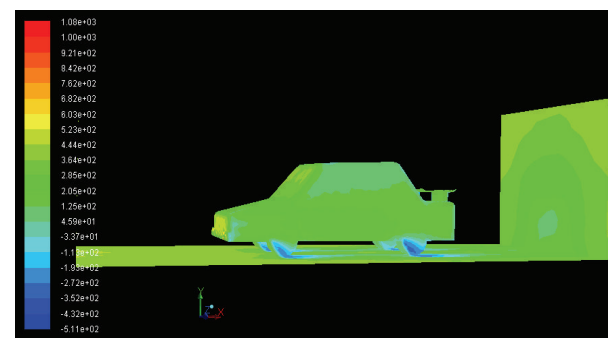

Figure 32: Total pressure contour on the car surface and road.

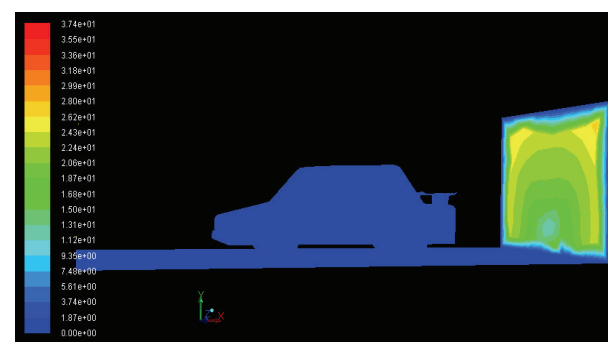

Figure 33: Velocity contour on car surface and road.

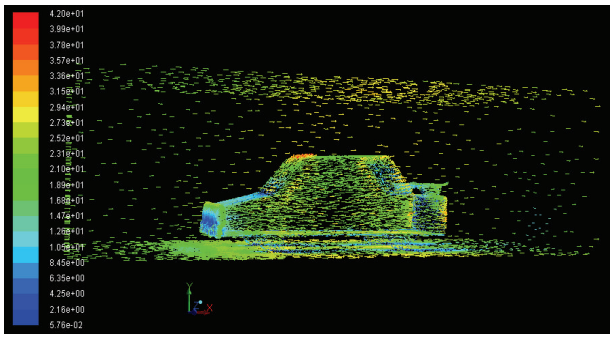

Figure 34: Velocity vector on car surface and symmetry.

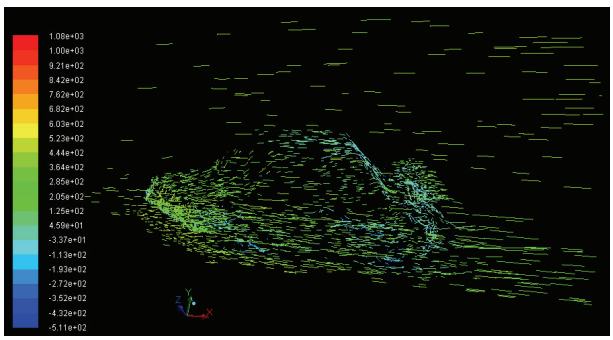

Figure 35: Pressure path lines on car surface and symmetry.

13. Simulation and Testing of Passenger Car with Tail Plates for Drag Coefficient and Lift Coefficient

In order to decrease the velocity of airflow from the underbody to the rear of the vehicle, a diffuser type tail plate was mounted at the rear of the vehicle as shown in Figure 36. A half-foot long plate was attached to the floor of the vehicle and a 5 cm long plate was attached to the top outer edge of the roof, both at 12-degree angle inclination.

Figure 37 shows the mesh generated on the surface of the model of generic passenger car with tail plates. The tetrahedron mesh is generated on its surface and a surface mesh of 1.5 mm size is created on the vehicle surface.

Figure 38 shows the total pressure distribution on the car surface, velocity inlet, pressure outlet, side wall, and on the road. The distribution of pressure on the front bumper is 2250 Pa and at the rear boot is 250 Pa.

The coefficient of drag and coefficient of lift are shown in Figures 39 and 40, respectively. The maximum value of the coefficient of drag (C_D) is 0.3376 and the maximum value of the coefficient of lift (C_L) is 0.1926.

Figures 41 and 42 are shows the static and absolute pressure distribution on the surface of the car.

Figure 43 shows the distribution of the pressure coefficient on the generic passenger car surface. The value of pressure coefficient on the front bumper is 3000 Pa and at the rear boot the value of the pressure coefficient is 50 Pa.

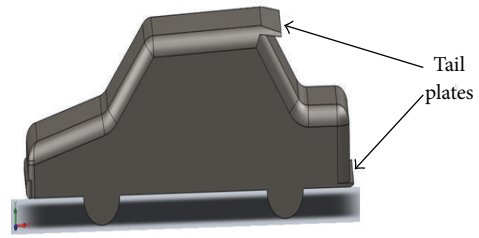

Figure 36: Passenger car with attached tail plates.

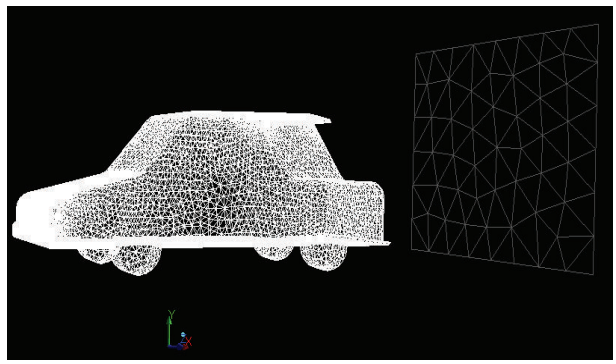

Figure 37: Meshed model of car with tail plates.

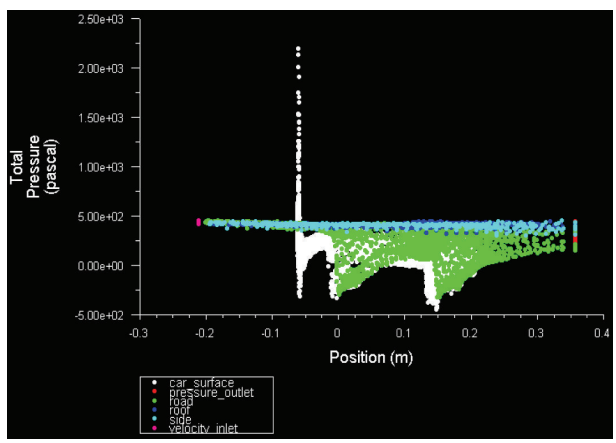

Figure 38: Total pressure distributions at car surface, pressure outlet, velocity inlet, and road.

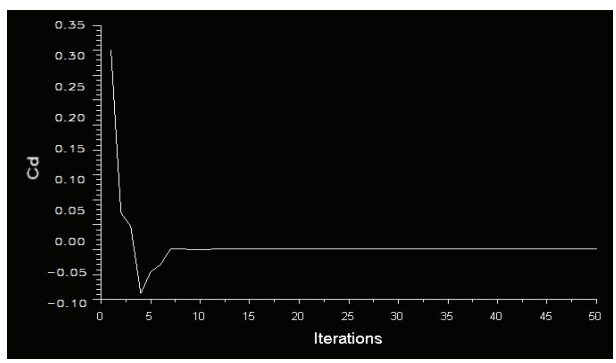

Figure 39: Coefficient of drag C_D of passenger car with tail plate.

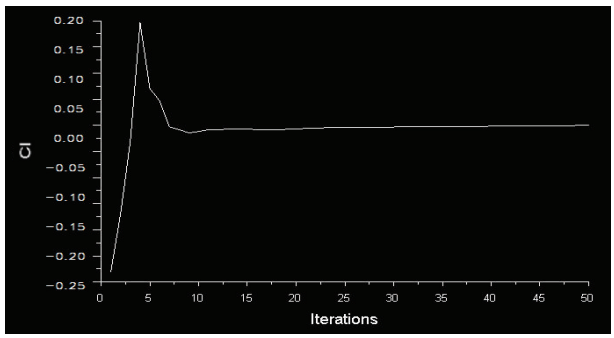

Figure 40: Coefficient of lift C_L of passenger car with tail plate.

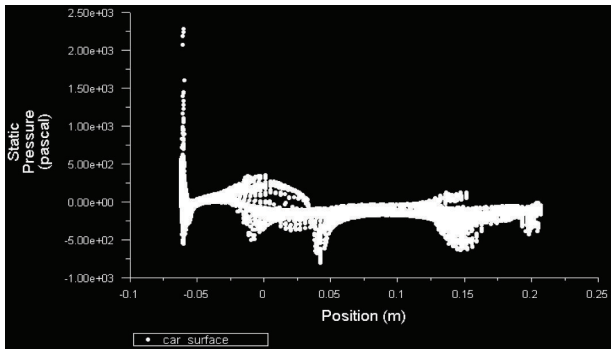

Figure 41: Static pressure distributions on car surface with tail plates.

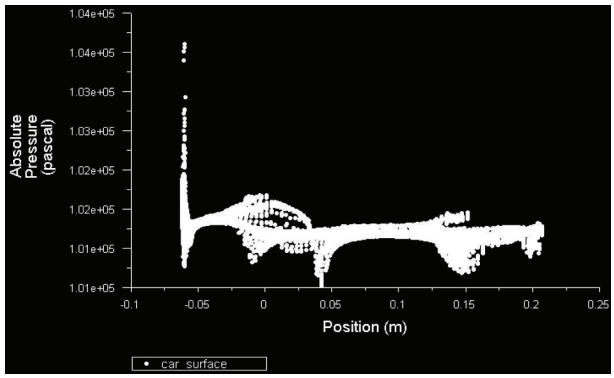

Figure 42: Absolute pressure distributions on car surface with tail plates.

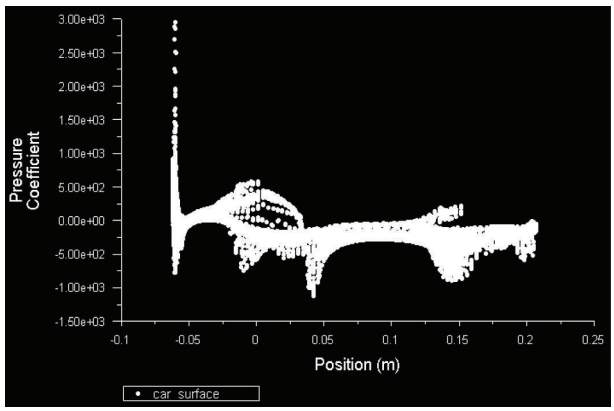

Figure 43: Pressure coefficient on car surface with tail plates.

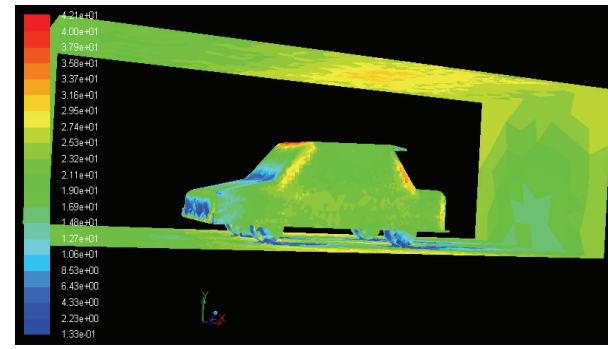

Figure 44: Total pressure contour on car surface, velocity inlet, pressure outlet, and road.

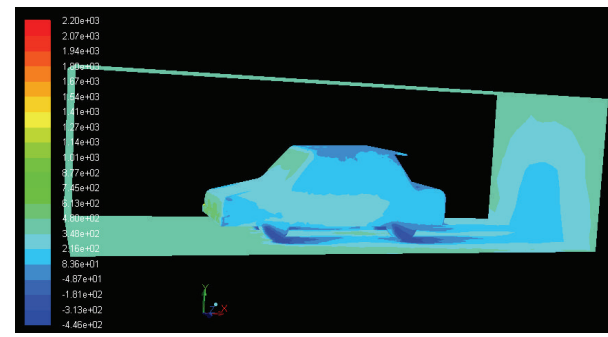

Figure 45: Velocity contour on car surface, velocity inlet, and pressure outlet.

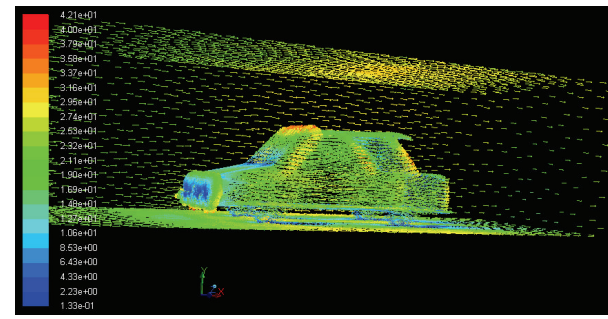

Figure 46: Velocity vector on car surface and symmetry.

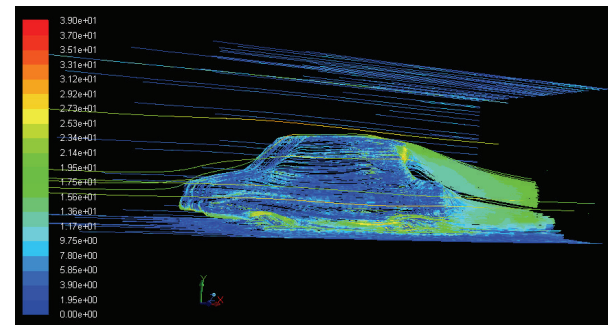

Figure 47: Pressure path lines on car surface and symmetry.

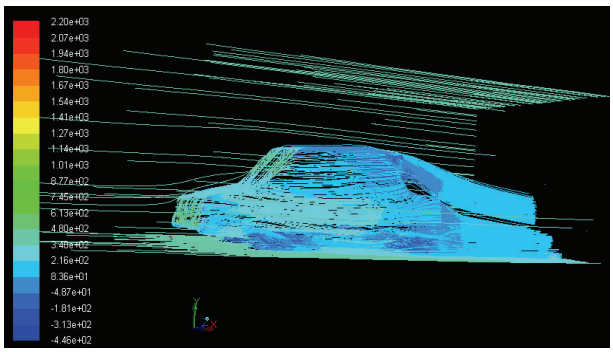

Figure 48: Velocity path lines on car surface and symmetry.

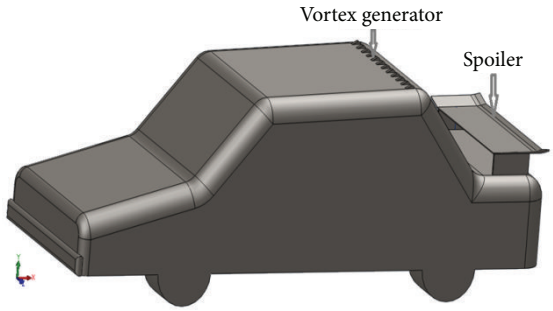

Figure 49: Passenger car with spoiler and vortex generators.

Total pressure contour and velocity contour are shown in Figures 44 and 45, respectively. The velocity magnitude vector and path lines are shown in Figures 46 to 48.

14. Simulation and Testing of Passenger Car Spoiler with Vortex Generators for Drag Coefficient and Lift Coefficient

In order to decrease the drag of the passenger car the combination of the add-on devices is applied on the car surface to overcome the drag coefficient of the car. Figure 49 shows the model of the passenger car with spoiler and vortex generators.

Figure 50 shows the mesh generated on the surface of the model of generic passenger car with spoiler and vortex generators. The tetrahedron mesh is generated on its surface and a surface mesh of 1.5 mm size is created on the vehicle surface.

Figure 51 shows the total pressure distribution on the car surface, velocity inlet, pressure outlet, side wall, and on the road. The distribution of pressure on the front bumper is 500 Pa and at the rear boot is 300 Pa.

The coefficient of drag and coefficient of lift are shown in Figures 52 and 53, respectively. The maximum value of the coefficient of drag (C_D) is 0.3359 and the maximum value of the coefficient of lift (C_L) is 0.1875.

Figure 54 shows the distribution of the pressure coefficient on the generic passenger car surface. The value of pressure coefficient on the front bumper is 100 Pa and at the rear boot the value of the pressure coefficient is −100 Pa (Figures 55, 56, and 57).

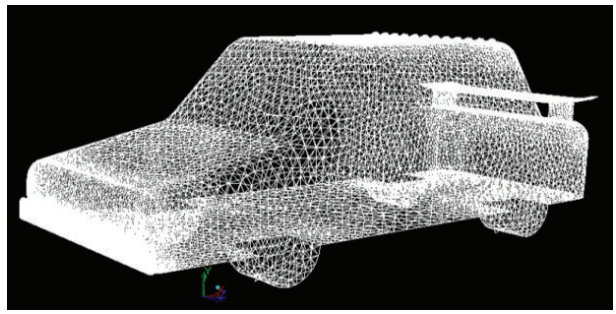

Figure 50: Meshed model of the passenger car with spoiler and vortex generators.

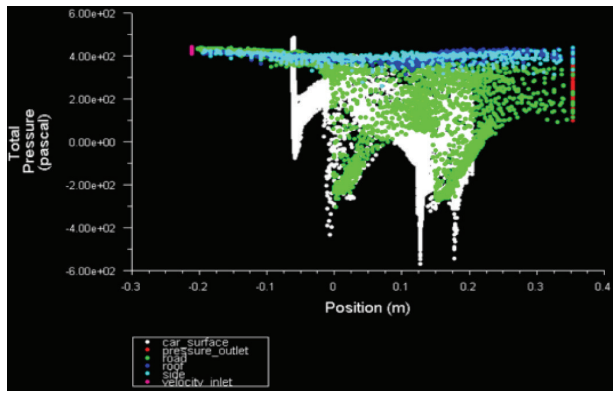

Figure 51: Total pressure distributions on the car surface, velocity inlet, pressure outlet, and on road.

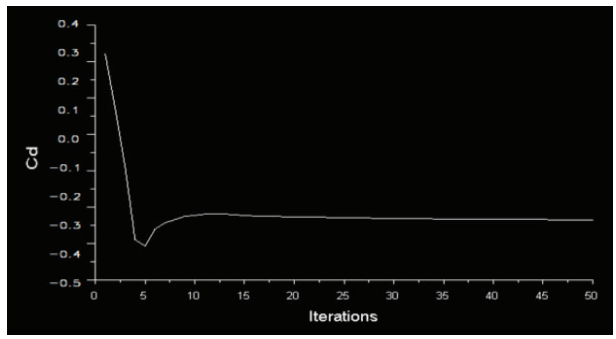

Figure 52: Coefficient of drag (C_D) passenger car with spoiler and VGs.

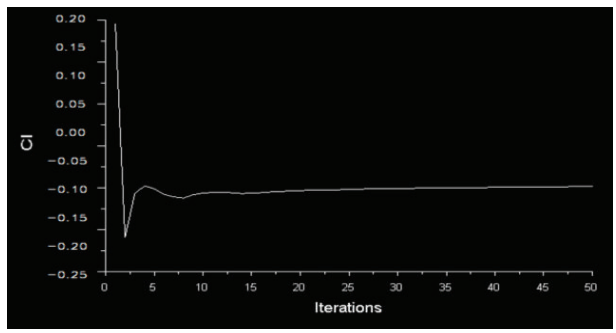

Figure 53: Coefficient of lift (C_L) passenger car with spoiler and VGs.

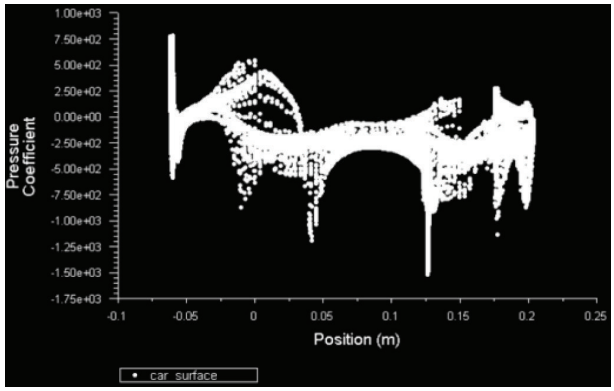

Figure 54: Pressure coefficient distributions on surface of the car with spoiler and VGs.

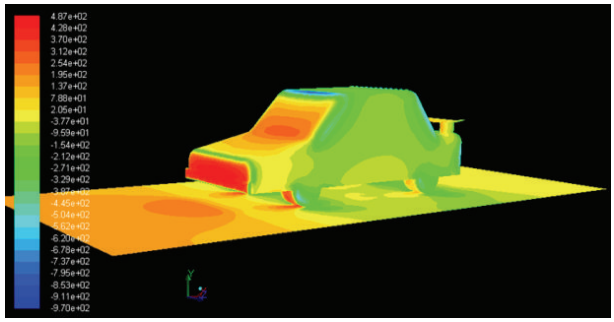

Figure 55: Static pressure contour on surface of car with spoiler and VGs.

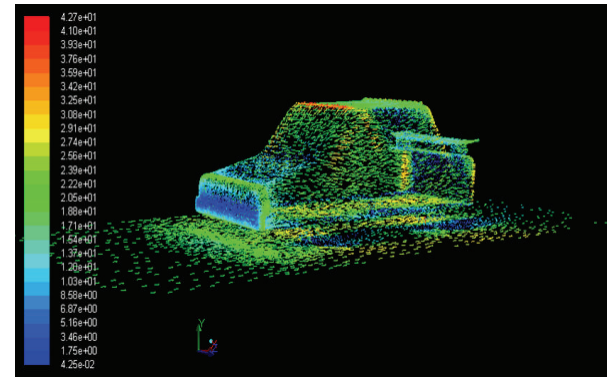

Figure 56: Velocity vector on surface of car with spoiler and VGs.

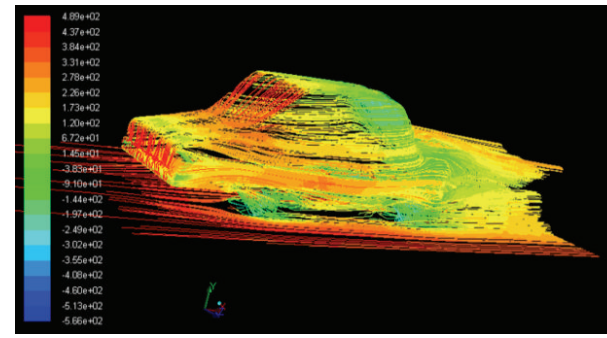

Figure 57: Total pressure path lines on surface of car with spoiler and VGs.

15. Result

In the above analysis there are different types of aerodynamic add-on devices used on the baseline car to get the results for the coefficient of drag and coefficient of lift.

In the first case the spoiler is applied on the boot of the passenger car with the inclination angle 12°. The coefficient of drag is 0.3441 and the coefficient of lift is 0.1985. The percentage reduction in drag coefficient in comparison with baseline car is 2.02% and in coefficient of lift is 6%. Hence, drag force and lift force on the passenger car are reduced as proportional to drag coefficient and lift coefficient, respectively.

In the second case the vortex generators are applied on the rear side at roof of the baseline car with inclination angle 12°. The coefficient of drag is 0.3471 and the coefficient of lift is 0.2085. The percentage reduction in drag coefficient in comparison with baseline car is 1.17% and in coefficient of lift is 9.8%. Hence drag force and lift force on the passenger car are reduced as proportional to drag coefficient and lift coefficient, respectively.

In the third case the tail plates are applied on the rear side: one is at the rear side of the roof garnish and the other is at the tail bumper of the passenger car. The coefficient of drag is 0.3376 and the coefficient of lift is 0.1926. The percentage reduction in drag coefficient in comparison with base line car is 3.87% and in coefficient of lift is 16.62%. Hence drag force and lift force on the passenger car are reduced as proportional to drag coefficient and lift coefficient, respectively.

In the fourth case the spoiler and VGs together are applied on the rear boot and rear side at the roof of the passenger car. The coefficient of drag is 0.3359 and the coefficient of lift is 0.1875. The percentage reduction in drag coefficient in comparison with base line car is 4.35% and in coefficient of lift is 18.83%. Hence, drag force and lift force on the passenger car are reduced as proportional to drag coefficient and lift coefficient, respectively.

From the above analysis, it is found that spoiler with VGs is more effective add-on device to reduce the drag coefficient and lift coefficient which are applied on the passenger car when the car is running on the road. The drag coefficients and drag forces are proportional to each other so when the drag forces are reduced, lift forces are also reduced because it is proportional to the lift coefficient. The comparative results between the baseline car and car with various add-on devices are shown in Table 9 and graphical representation in Figures 58 and 59, respectively.

16. Conclusion

Computational fluid dynamics (CFD) simulations of the steady flow field around passenger car models with and without add-on devices both were presented comparing the simulated data to each other. The ANSYS Fluent with the

Table 9: Drag and lift coefficient of all add-on devises.

Configurations	Drag coefficient	% C_D reduction from baseline	Lift coefficient	% C_L reduction from baseline
Baseline	0.3512	0	0.2310	0
Vortex generators	0.3471	1.17	0.2085	9.8
Spoiler	0.3441	2.02	0.1985	6
Tail plates	0.3376	3.87	0.1926	16.62
Spoiler with vortex Generators	0.3359	4.35	0.1875	18.83

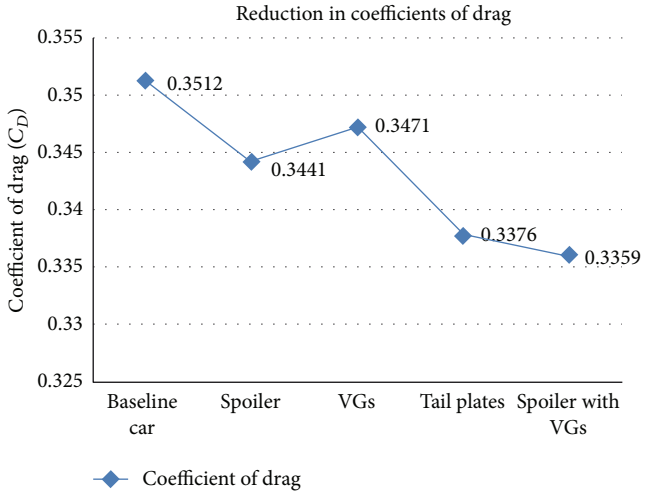

Figure 58: Graphical presentation of reduction of drag coefficients.

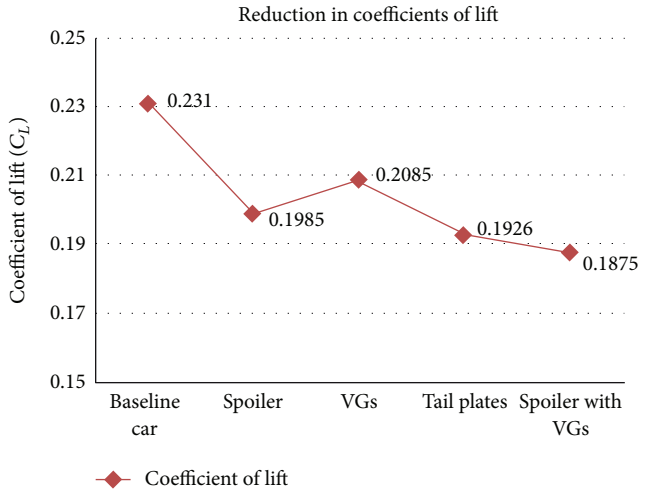

Figure 59: Graphical presentation of reduction of lift coefficients.

k-ε steady model is used for the simulations of aerodynamics. In this analysis, the coefficient of drag has been reduced up to 4.35% and coefficient of lift is reduced up to 18.83% due to the addition of spoiler with VGs. Hence, the spoiler with VGs is the effective tool to reduce the drag force on vehicle.

The effects of different aerodynamic add-on devices on flow and its structure over a generic passenger car may be analysed using CFD approach. The objective is to reduce aerodynamic drag acting on the vehicle and thus improve the fuel efficiency of passenger car. Hence, the drag force can be reduced by using add-on devices on vehicle and fuel economy, and stability of a passenger car can be improved.

Conflict of Interests

The authors declare that there is no conflict of interests regarding the publication of this paper.

References

[1] A. Gilhaus and R. Hoffmann, "Directional stability," in *Aerodynamics of Road Vehicles*, W. H. Hucho, Ed., SAE International, Warrendale, Pa, USA, 1998.

[2] J. R. Callister and A. R. George, "Wind noise," in *Aerodynamics of Road Vehicles*, W. H. Hucho, Ed., SAE International, Warrendale, Pa, USA, 1998.

[3] F. R. Bailey and H. D. Simon, "Future directions in computing and CFD," AIAA Paper 92-2734, 1992.

[4] H. Taeyoung, V. Sumantran, C. Harris, T. Kuzmanov, M. Huebler, and T. Zak, "Flow-field simulations of three simplified vehicle shapes and comparisons with experimental measurements," *SAE Transactions*, vol. 106, pp. 820–835, 1996.

[5] *Fluent 6.1 User's Guide*, Fluent, Lebanon, NH, USA, 2003.

[6] *TGrid 3.4 User's Guide*, Fluent, Lebanon, NH, USA, 2001.

[7] K. Ahmad, M. Khare, and K. K. Chaudhry, "Model vehicle movement system in wind tunnels for exhaust dispersion studies under various urban street configurations," *Journal of Wind Engineering and Industrial Aerodynamics*, vol. 90, no. 9, pp. 1051–1064, 2002.

[8] Z. Yang and B. Khalighi, "CFD simulation for flow over pickup trucks," SAE Paper 2005-01-0547, 2005.